Received: 10 March 2017 | Revised: 2 May 2017 | Accepted: 3 May 2017

DOI: 10.1111/cbdd.13027

RESEARCH ARTICLE

WILEY

# Pyrimidine containing epidermal growth factor receptor kinase inhibitors: Synthesis and biological evaluation

**Gaurav Joshi**[1] | **Himanshu Nayyar**[1] | **Sourav Kalra**[2] | **Praveen Sharma**[2] | **Anjana Munshi**[2] | **Sandeep Singh**[2] | **Raj Kumar**[1]

[1]Laboratory for Drug Design and Synthesis, Centre for Pharmaceutical Sciences and Natural Products, Central University of Punjab, Bathinda, India

[2]Centre for Human Genetics and Molecular Medicine, Central University of Punjab, Bathinda, India

**Correspondence**
Raj Kumar, Laboratory for Drug Design and Synthesis, Centre for Pharmaceutical Sciences and Natural Products, Central University of Punjab, Bathinda, India.
Emails: raj.khunger@gmail.com; rajcps@cup.ac.in

**Funding information**
University Grants Commission, Grant/Award Number: F.30-13/2013(BSR); Science and Engineering Research Board, Grant/Award Number: SR/SO/AS-31/2014

Structure-based design and synthesis of pyrimidine containing reversible epidermal growth factor receptor (EGFR) inhibitors **1a–d** are reported. The compounds (**1a–d**) inhibited the EGFR kinase activity in vitro with $IC_{50}$ range 740 nM to 3 μM. mRNA expression of EGFR downstream target genes, that is twist, c-fos and aurora were found to be altered upon treatment with compounds **1a–d**. The compounds **1a–d** exhibited excellent anticancer activity at low micromolar level (3.2–9 μM) in lung, colon and breast cancer cell lines. Furthermore, compounds induced the alteration in mitochondrial membrane potential and reactive oxygen species level and. Selected compound **1b** was found to increase sub-G1 population indicative of cell death, the mode of cell death was apoptotic as evident from Annexin V verses propidium iodide assay. Molecular modelling further helped to investigate the binding recognition pattern of the compounds in ATP binding EGFR domain similar to erlotinib and dissimilar to WZ4002.

**KEYWORDS**
anticancer, cell cycle analysis, EGFR, molecular modelling, pyrimidine

## 1 | INTRODUCTION

Cancer involves the uncontrolled proliferation of the cells and can occur almost in any type of tissue.[1] Cancerous cells possess certain characteristics that include tissue invasion, metastasis, evasion of apoptosis, angiogenesis, inflammation, immortality which make them insensitive to conventional anticancer agents.[2–4] This necessitated the need of target-based anticancer drug discovery.[5] Amongst the various anticancer drug targets known, epidermal growth factor receptor (EGFR) belonging to a family of tyrosine kinase, discovered by Stanley and Cohen is well characterized and most studied due to its overexpression in a variety of cancer especially lung, breast, ovary, etc. and autophosphorylation leading to upregulated downstream cell signalling.[6]

Quinazoline-based first-generation EGFR inhibitors (Figure 1) such gefitinib and erlotinib were approved by USFDA in 2002 and 2004, respectively against non-small cell lung cancer (NSCLC).[7] However, the emergence of acquired resistance and point mutations (T790M and L858R) with their use made them ineffective and to overcome this, development of second-generation EGFR inhibitors such as canertinib and afatinib able to make a covalent bond with CYS797 took place.[8–10] But, due to their skin and gastrointestinal toxicity[11]; possibly because of their similar quinazoline scaffold and covalent bond formation stimulated the researchers to explore another alternate template, that is pyrimidine-based irreversible, third-generation EGFR inhibitors for instances WZ4002 and osimertinib.[12,13] However, early Phase I clinical trials of third-generation EGFR inhibitors are found to be promising and effective, but they are likely to produce off-target side-effects and toxicities after their prolonged use.[14,15]

Thus, based on our previous experiences in anticancer drug discovery,[16–24] we have designed the target compounds (Figure 2) considering the common

  

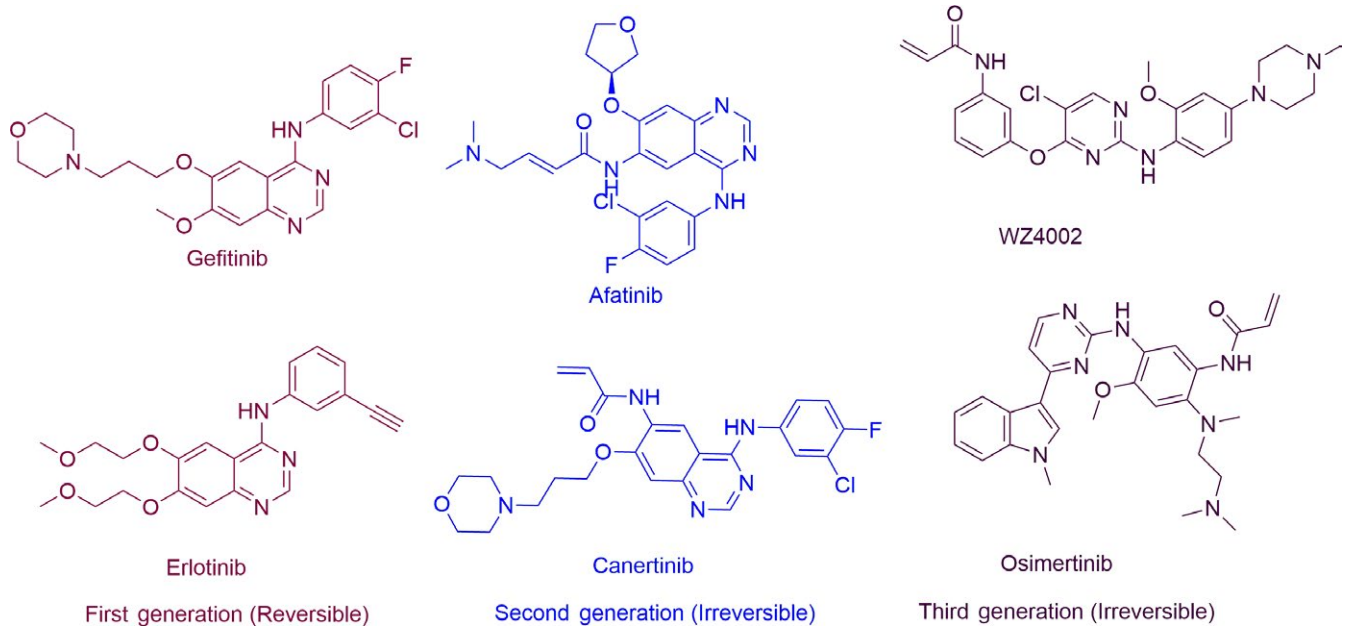


**FIGURE 1** Chemical structures of some reported epidermal growth factor receptor inhibitors

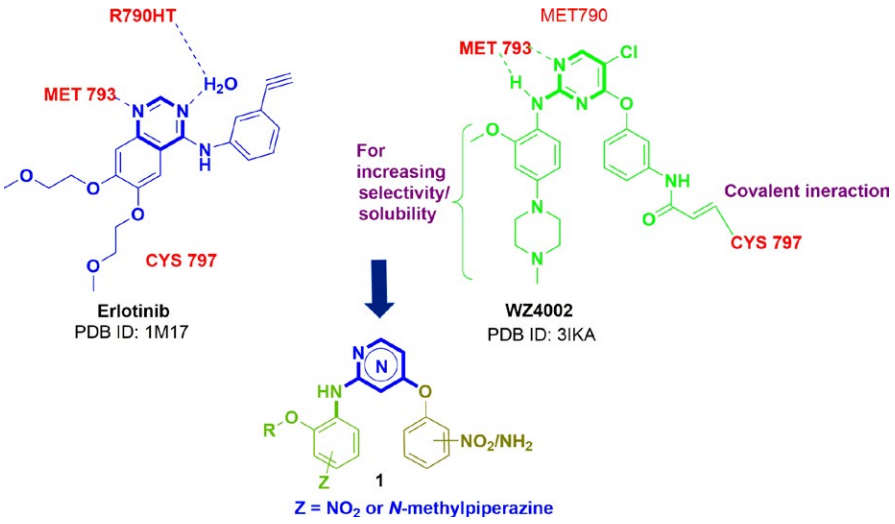


**FIGURE 2** Design of target compounds (**1**) as epidermal growth factor receptor inhibitors

pharmacophoric features of erlotinib (reversible) and WZ4002 (irreversible)[25] with the assumptions that compounds should: (a) possess pyrimidine ring with 2-alkoxy/hydroxyl aniline moiety for hydrogen bond interaction with MET793, (b) be able to selectively target hypoxic tumours by possessing nitro substituent on either or both the aromatic rings with/without solubility enhancer due to their bioreduction to yield electrophilic substances which are capable of damaging protein and nucleic acids[24,26] and have radiosensitizing ability,[27] (c) be reversible and non-covalent in nature as irreversible inhibitors not only make covalent interactions with CYS797 of target but also undergo conjugate addition with other nucleophiles in the body due to their Michael acceptor property, thereby leading to off-target side-effects and, (d) be easy to synthesize and cost-effective.

In the present work, synthesis and detailed in vitro biological evaluation of the target compounds are reported. Additionally, mechanistic interventions derived through target based EGFR inhibitory activities, reactive oxygen species generation, mitochondrial destabilization potential, the effect of EGFR inhibition on its down regulatory mRNA levels through RT-PCR, followed by the arrest of the cell cycle with respect to synthetics has been performed. The facts were further substantiated through molecular docking methods on kinase domain of EGFR.

## 2 | EXPERIMENTAL SECTION

### 2.1 | General

All the reagents required for synthesis were purchased Sigma-Aldrich, Loba, Avra and CDH, India and were used without further purification. All the reagents for biology were purchased from Sigma, Invitrogen and cells were procured from NCCS Pune, India. Flow cytometry experiments were performed in BD ACCURI C6 software, and all the absorbance/fluorescent-based studies were performed on a Biotage microplate reader.

All yields refer to isolated products after purification. Products were characterized by spectroscopic data (IR, NMR, MS spectra and CHNS analysis). NMR experiments were measured in $CDCl_3$/d6-DMSO relative to TMS (0.00 ppm). IR (KBr pellets) spectra were recorded on a Fourier transform infrared (FT-IR) Thermo spectrophotometer. Melting points were determined in open capillaries and were uncorrected. All the target compounds were characterized by IR, NMR, and Mass and/or elemental analyses (see Supplementary information).

### 2.2 | Chemistry

#### 2.2.1 | Synthesis of 2-chloro-4-(3-nitrophenoxy)pyrimidine (4)

A mixture of 2, 4-dichloro pyrimidine (0.5 g, 3.35 mmol), 3-nitrophenol (0.46 g, 3.35 mmol) and NaOH (0.134 g, 3.35 mmol) in acetone and water (3 ml v/v) was stirred at 60°C for 24 hr. The completion of the reaction was observed by TLC. The reaction mixture was then allowed to cool down to room temperature and excess of solvent was removed using rotary evaporator. Dried compound was washed with a solution of 10% sodium carbonate (25 ml × 3) and dried over anhydrous $Na_2SO_4$ to afford the crude product which was used next step without further purification.

#### 2.2.2 | Synthesis of 2,4-bis(3-nitrophenoxy) pyrimidine (1a)

A mixture of 2, 4-dichloro pyrimidine (0.5 g, 3.35 mmol), 3-nitrophenol (0.92 g, 6.70 mmol) and NaOH (0.134 g, 3.35 mmol) in acetone and water (3 ml v/v) was stirred at 60°C for 48 hr. The progress of the reaction was monitored by TLC. The reaction mixture was then allowed to cool down to room temperature and excess of solvent was removed using rotary evaporator. Dried compound was washed with a solution of 10% sodium carbonate (25 ml × 3) and further dried over anhydrous $Na_2SO_4$ to afford the crude product. The purity of the isolated **1a** was determined by HPLC (Shimadzu) (C18, 4.6 × 250 mm, 5 μm), using 25% MeOH as mobile phase with a flow rate of 1.0 ml/min. The physical data of **1a** has been given in Supplementary information.

#### 2.2.3 | Synthesis of 1-(3-methoxy-4-nitrophenyl)-4-methylpiperazine (8)

1-methyl piperazine (0.42 ml, 4.378 mmol) and 4-fluoro 2-methoxy 1-nitrobenzene (0.5 g, 2.91 mmol) were heated at 50°C for 4–6 hr in DMF and $K_2CO_3$ (2 eq., 0.80 g). After the completion of the reaction (TLC), the crude mixture was extracted with ethyl acetate (10 ml × 3). The organic layer was evaporated using a rotary evaporator to afford yellow colour compound.

#### 2.2.4 | Synthesis of 2-methoxy-4-(4-methylpiperazin-1-yl) aniline (5)

To a solution of **8** (1.99 mmol, 0.5 g) in methanol (3 ml) was added tin (II) dichloride dihydrate (9.95 mmol 2.25 g). The reaction mixture was allowed to cool and conc. HCl was added (4 ml). The reaction was stirred further at room temperature for 6–8 hr. After the completion of the reaction (TLC), excess solvent was removed using rotary evaporator. The dried compound was washed and basified using conc. NaOH (pH 11). The water layer was extracted with diethyl ether (25 ml × 3). The combined organic layer was dried ($Na_2SO_4$), filtered and the solvent was removed under reduced pressure to afford the title compound (**5**).

#### 2.2.5 | Synthesis of *N*-(2-methoxy-4-(4-methylpiperazin-1-yl) phenyl)-4-(3-nitrophenoxy) pyrimidin-2-amine (1b)

**4** (0.5 g, 1.9 mmol) and **5** (0.36 g, 1.6 mmol) were dissolved in isobutanol and $CF_3COOH$ (1.6 ml, 1.05 mmol) was added. The reaction mixture was refluxed for 3 hr. After the completion of the reaction (TLC), the crude mixture was extracted with methylene chloride (10 ml × 3). The organic layer was evaporated using rotary evaporator to obtain a brownish colour solid that was purified through column chromatography (Silica gel #60-120, 70%–30% EtOAc: Petroleum ether) to obtain the pure product. The purity of the isolated **1b** was determined by HPLC (Shimadzu) (C18, 4.6 × 250 mm, 5 μm), using 30% MeOH as mobile phase with a flow rate of 1.0 ml/min. The physical data of **1b** has been given in Supplementary information.

#### 2.2.6 | Synthesis of 2-((4-(3-nitrophenoxy) pyrimidin-2-yl)amino)phenol (1c)

**4** (0.5 g, 1.9 mmol) and **5** (0.4 g, 1.80 mmol) in DMF and $K_2CO_3$ (2 eq.) were heated at 50°C for 5 hr. After the completion of the reaction (TLC), the crude mixture was extracted with ethyl acetate (10 ml × 3). The organic layer was evaporated using a rotary evaporator to afford a solid compound. The product was purified through column chromatography (Silica gel #60-120, 20%–80%

EtOAc: Petroleum ether) to obtain the pure product (**1c**). The purity of the isolated **1c** was determined by HPLC (Shimadzu) (C18, 4.6 × 250 mm, 5 μm), using 25% MeOH as mobile phase with a flow rate of 1.0 ml/min. The physical data of **1c** has been given in Supplementary information.

### 2.2.7 | Synthesis of 2-((4-(3-aminophenoxy) pyrimidin-2-yl)amino)phenol (1d)

**1c** (0.5 g, 2.21 mmol) was dissolved in methanol (3 ml), and to it, tin (II) dichloride dihydrate (9.95 mmol 2.25 g) was added. The reaction mixture was allowed to cool and conc. HCl was added (4 ml). The reaction was stirred further at room temperature for 6–8 hr. After the completion of the reaction (TLC), excess solvent was removed using rotary evaporator. The dried compound was washed and basified using conc. NaOH (pH 11). The water phase was extracted with diethyl ether (25 ml × 3). The combined organic layer was dried ($Na_2SO_4$), filtered dried and purified by column chromatography (Silica gel #60-120, 60%–40% EtOAc: Petroleum ether) to obtain the pure product (**1d**). The purity of the isolated **1d** was determined by HPLC (Shimadzu) (C18, 4.6 × 250 mm, 5 μm), using 25% MeOH as mobile phase with a flow rate of 1.0 ml/min. The physical data of **1d** has been given in Supplementary information.

## 2.3 | Molecular docking studies

The protein structure PDB ID: 1M17[28] was procured from the protein data bank. It has better resolution of 2.6 angstroms and contains co-crystallized erlotinib. The ligands were prepared using OPLS-2005 force field in the Ligprep module. The protein preparation was done using the "Prepwiz" module in which addition of hydrogen atoms, bond orders assignment, removal of water molecules beyond 5 Å and filling the missing side chain and loops using PRIME module was done. The preprocessed protein was further refined using the OPLS-2005 force field. The grid generation was carried out using grid generation module considering the centroid of the co-crystallized ligand erlotinib. The docking was performed using GLIDE module with extra precision (XP) mode.

## 2.4 | Biology

### 2.4.1 | EGFR inhibitory assay

EGFR Inhibitory potential of the investigational compounds was determined by z-lyte kinase assay kit-tyr4 peptide (catalogue no. PV3193). The inhibitory effect on kinase was measured spectrophotometrically at 400, 445 and 520 nm, respectively. Erlotinib was used as a positive control for the inhibitory assay. For assay mixture consist of 133 μl kinase buffer, 0.5 μl kinase peptide mixtures, 0.5 μl phosphopeptide mixtures, 0.5 μl ATP test sample solution. The investigational compounds were serially diluted at a concentration of 250, 750 nM and 1, 5, 25 μM in 4% DMSO. The assay plates were prepared in triplicates and were mixed and incubated at room temperature for 1 hr. After this treatment with 5 μl of development, the solution was done and further kept in dark for another 1 hr. Ultimately the enzymatic reaction was stopped with the addition of 5 μl stop solution. The absorbance was measured using UV–VIS spectrophotometer.

Calculation emission ratio: Emission ratio = Coumarin Emission (445 nm)/fluorescein emission (520 nm). The extent of phosphorylation was calculated by following formula:

$$\%\ \text{phosphorylation} = 1 - \frac{(\text{Emission rate} \times F100\%) - C100\%}{(C0\% - C100\%) + [\text{Emission rate}(F100\% - F0\%)]}$$

where C0% = average coumarin emission signal of the 100% Phos. Control; C100% = average coumarin emission signal of the 0% Phos. Control; F100% = average Fluorescein emission signal of the 100% Phos. Control; F0% = average Fluorescein emission signal of the 0% Phos. Control.

### 2.4.2 | RT-PCR assay

RNA was isolated from cells using Tri-reagent available with Sigma-Aldrich and was in accordance with manufacturer's protocol. Cells were lysed using Tri-reagent and then mixed with chloroform and further centrifuged at 12,000 *g* for 10 min. The aqueous phase was removed and precipitation of RNA was done using isopropanol. The precipitates were further pelleted at 7952 *g* for 10 min. The pellet was air-dried and suspended in ultrapure water.

One microgram RNA as template was used to synthesize cDNA in presence of MMLV-RT, MMLV-RT buffer, 10 mM dNTPs, DTT and RNAse OUT (Invitrogen).

The list of primer used for RT and real-time PCR is given below:

c-Fos (Fwd) - 5′ aaggagaatccgaagggaaa
c-Fos (Rev) - 5′ agggcccttatgctcaatct
Twist (Fwd) - 5′ gtccgcagtcttacgaggag
Twist (Rev) - 5′ ccagcttgagggtctgaatc
Actin (Fwd) - 5′ agagctacgagctgcctgac
Actin (Rev) - 5′ agcactgtgttggcgtacag
Aurora-A (Fwd) - 5′ ctcgccaggtaaacagaagc
Aurora-A (Rev) - 5′ ccttagttcgcctctgcatc

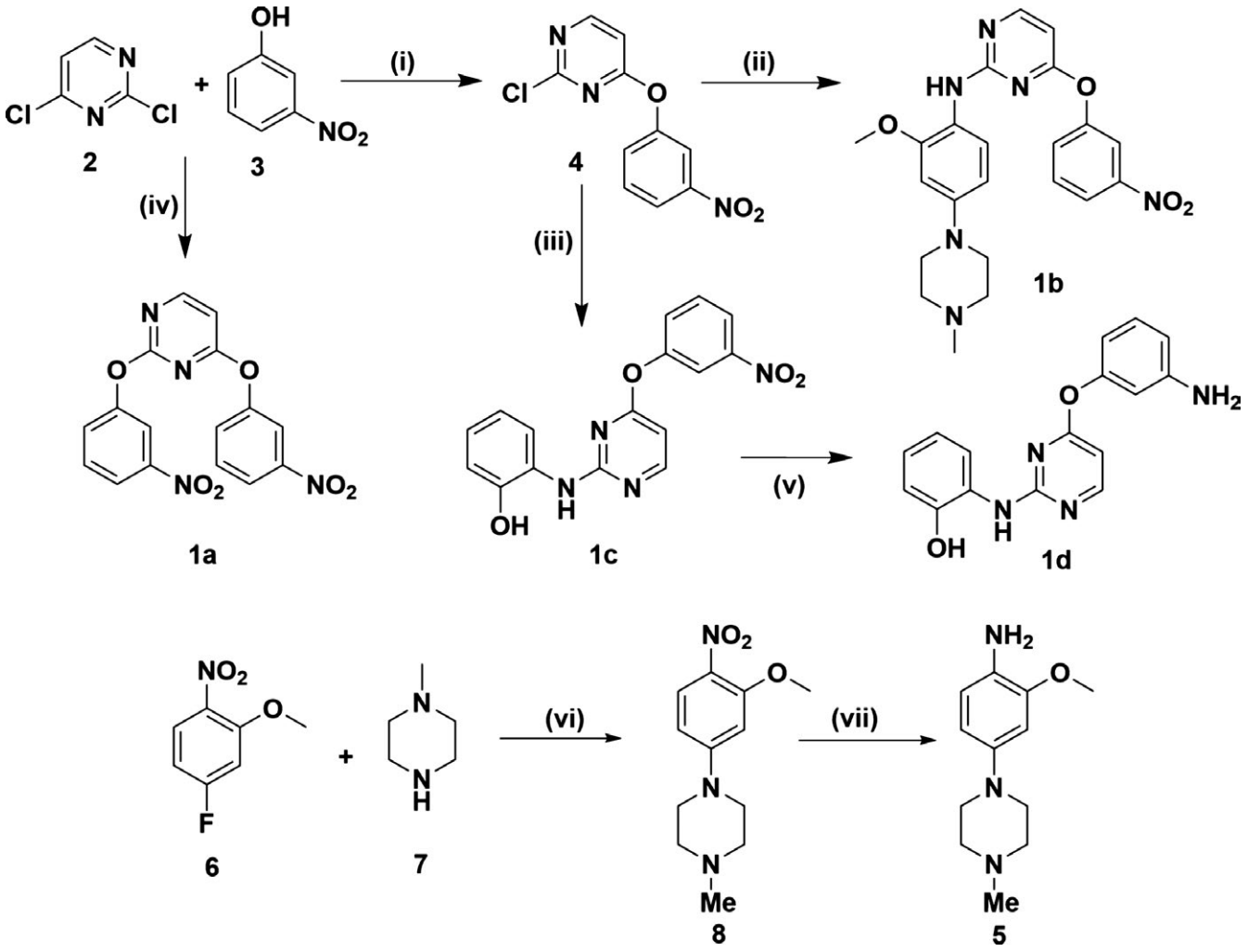


**SCHEME 1** Synthesis of target compounds (**1a–d**). Reaction conditions: (i) acetone-water, 60°C, 24 hr, 94%; (ii) isobutanol, $CF_3COOH$, 100°C, 3 hr, 62%; (iii) DMF, $K_2CO_3$, 50°C, 5 hr, 60%; (iv) acetone-water, 60°C, 48 hr, 83%; (v) $SnCl_2$ (3–4 equiv), conc. HCl, 6–8 hr, 71%; (vi) *N*-methyl-piperazine, $K_2CO_3$, DMF, 50°C, 4–6 hr, 93%, (vii) $SnCl_2$ (3–4 equiv), conc. HCl, 6–8 hr, 73%

### 2.4.3 | 3-(4,5-dimethythiazol-2-yl)-2,5-diphenyl tetrazolium bromide (MTT) assay

Antiproliferative potential of the investigational compounds was assessed using MTT assay. The assay was performed in 96-well plate in which each well was filled with 100 µl complete cell suspension media to which treatment with the synthetic compounds was given at three concentrations viz., 1, 5 and 25 µM and incubated thereafter for 24 hr. After 24 hr, media was discarded and subsequently washed with 1× PBS and was consequently treated with MTT dye (5 mg in 10 ml of 1× PBS) at a concentration of 10 µl per well and incubated at room temperature in dark for 4 hr to allow the formation of formazan crystals. After that formazan crystals were dissolved in DMSO and the absorbance was read spectrophotometrically using microplate reader at 570 nm. The results were then represented as mean ± *SD* obtained from three independent experiments.

### 2.4.4 | Human peripheral blood mononuclear cells (PBMCs), Buccal cell culture and MTT assay

Blood from healthy volunteer was drawn and treated with RBC lysis buffer to isolate hPBMCs. The cells were then suspended in RPMI media supplemented with 10% foetal Bovine serum (FBS), 1× antibiotic solution. The suspension was added to 96 well plate (10,000 cells per well) at 100 µl and was incubated at 37°C. The treatment with the synthetic compounds was given at three concentrations viz., 5 and 25 µM and incubated thereafter for 24 hr and were consequently treated with MTT dye (5 mg in 10 ml of 1× PBS) at a concentration of 10 µl per well and incubated at room temperature in dark for 4 hr to allow formation of formazan crystals. After that formazan crystals were dissolved in DMSO and the absorbance was read spectrophotometrically using microplate reader at 570 nm. The results were then represented as mean ± *SD* obtained from three

**TABLE 1** EGFR inhibitory activity of the investigational compounds **1a–d**

| Compound name | EGFR inhibitory activity; $IC_{50}$[a] |
|---|---|
| **1a** | 3 ± 0.65 μM |
| **1b** | 740 ± 0.6 nM |
| **1c** | 4 ± 0.91 μM |
| **1d** | 750 ± 0.32 nM |
| Erlotinib | 195 ± 0.46 nM |

[a]Values are derived from averaging three independent experiments and each experiment was performed in triplicate.

independent experiments. Buccal cavity cells used during the experiment were harvested and culture according to the earlier described protocol by Weisberg et al.[29,30] All human cell-based experiment was conducted in accordance with protocol no. CUPB/cc/14/IEC/4,483 approved by Institutional Ethics Committee of Central University of Punjab, Bathinda, as per guidelines issued by Indian Council of Medical Research (ICMR), Govt. of India.

### 2.4.5 | Reactive oxygen species (ROS) and mitochondrial membrane integrity assays

Cancer cells were treated with the investigational compounds. 24 hr post-treatment, the cells were processed for JC-1 and DHE staining to study mitochondrial membrane polarization and ROS generation, respectively. DHE analysis was carried out in flow cytometer (BD Accuri) (for single cell analysis), and also by measuring OD at 610 nm using a microplate reader. JC-1 assay analysis was carried out by measuring OD at (emission at 527 and 590) using a microplate reader. The experiments were performed at 37°C followed by washing with 1× PBS to remove the extra dye.

### 2.4.6 | Cell apoptosis assay and mode of cell death (using Annexin V and Propidium Iodide)

Cellular samples (A549 previously treated with compound **1b** for 24 hr) were prepared for staining by transferring $1 \times 10^6$ cell per tube. The cells were further centrifuged at 115 *g* for 5 min and washed with 1× PBS. Thereafter cells were fixed using chilled ethanol and incubated for 3 hr at −20°C. Post 3 hr cells were subjected to centrifugation at 495 *g* and washed once with 1× PBS. 50 μl of propidium iodide (along with 50 μl Ribonuclease A) was added to each well and incubated for 30 min at room temperature in dark. The DNA content was then measured using Flow cytometer (BD Accuri).

To investigate the exact mode a cell death, Annexin V vs propidium iodide assay was performed. The cancer cell lines treated with investigational compound **1b** previously for 24 hr were harvested and to each tube added Annexin V dye and propidium iodide (above-mentioned steps were repeated) and incubated for 30 min at room temperature in the dark.

## 3 | RESULTS AND DISCUSSION

### 3.1 | Synthesis

Synthesis of the target compounds (**1a–d**; Scheme 1) was accomplished by heating 2, 4-dichloro pyrimidine (**2**; 1 equiv) with 3-nitrophenol (**3**; 2 equiv) at 60°C in the acetone-water mixture under basic condition (sodium hydroxide) for 24 hr that regioselectively afforded **4**. However, the complete $S_NAr$ occurred when **2** (1 equiv) was reacted with **3** (2 equiv) and **4** when treated with **5** at 100°C in isobutanol under the catalytic influence of $CF_3COOH$ for 3 hr yielded **1b**. The compound **5** was synthesized from **6** using the reported procedure.[31] Interestingly, **4** when heated with **5** in DMF at 50°C in the presence of $K_2CO_3$ for 5 hr, resulted in the formation of **1c**, a methyl ether as well as *N*-methylpiperzinyl cleaved product. However, deprotection of methyl ether under basic conditions is known but to the best of our knowledge cleavage of *N*-methylpiperzinyl is unreported. Compound **1c** underwent reduction of the nitro group to afford **1d** in methanol when treated with $SnCl_2$ (3–4 equiv) and concentrated hydrochloric acid for 6–8 hr.

All the final compounds were purified by column chromatography and were unreported and fully characterized by mp, IR, NMR, Mass and or elemental analyses (see Supplementary information).

### 3.2 | Biological evaluation

#### 3.2.1 | EGFR kinase inhibitory activity

To investigate EGFR inhibitory potential, investigational compounds (**1a–d**) were screened for inhibition of ATP-dependent phosphorylation of EGFR and inhibitory potential was measured spectrophotometrically at 400, 445 and 520 nm respectively. Erlotinib was used as a positive control for the inhibition test. The assay relies upon an enzymatic reaction through which autophosphorylation and signalling activity of the EGFR is measured.[17] The results are summarized in Table 1. Compounds **1b** and **1d** showed activities in nanomolar range in accordance with erlotinib, whereas compounds **1a** and **1c** exhibited low micromolar activity.

#### 3.2.2 | RT-PCR assay

EGFR signalling is a growth promoting signalling that ensures cell survival as well as proliferation via modulation of target gene expression. As the synthesized compounds

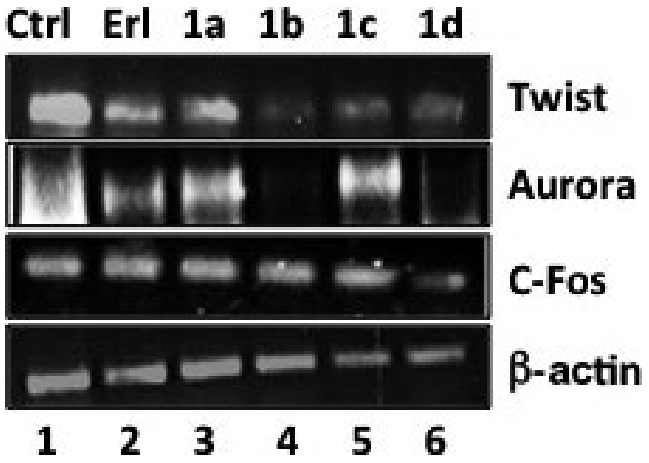


**FIGURE 3** RT-PCR showing Twist, Aurora and c-Fos alongside loading control β-actin after treatment with compounds as indicated while Erlotinib (Erl) is used as positive control

are designed to target EGFR, we proceeded to analyse the mRNA expression of EGFR target genes, twist, c-Fos as well as aurora. EGFR is known to up-regulate expression of twist as well as aurora to exert anti-apoptotic effect,[17,32] while it down-regulates the expression of c-Fos, which is apoptotic in nature.[17,32] Briefly, A549 cells were treated with designed EGFR inhibitors (at 5 μM of concentration) and Erlotinib was used as positive control for its inhibition followed by RT-PCR-based analysis of above-mentioned target gene expression. The results showed that twist expression was down-regulated upon treatment with **1b**, **1c** and **1d**, as well as erlotinib (Figure 3 lane 2 of 4) compared to the control cells while Aurora expression was downregulated by compounds **1b** and **1d**. On the other hand, same treatments lead to up-regulation of c-Fos expression (Figure 3, lane 2–4) compared to the control cells. As c-Fos is negatively regulated by EGFR, it may be concluded from our results that compounds **1b** and **1d** were able to inhibit EGFR activity which leads to down-regulation of twist and up-regulation of c-Fos expression while aurora, which is also a target of EGFR kinase, expression remained unchanged. β-Actin was used as loading control for all the expression studies.

### 3.2.3 | Molecular docking

As designed compounds were able to inhibit EGFR kinase activity, a molecular docking of all the compounds

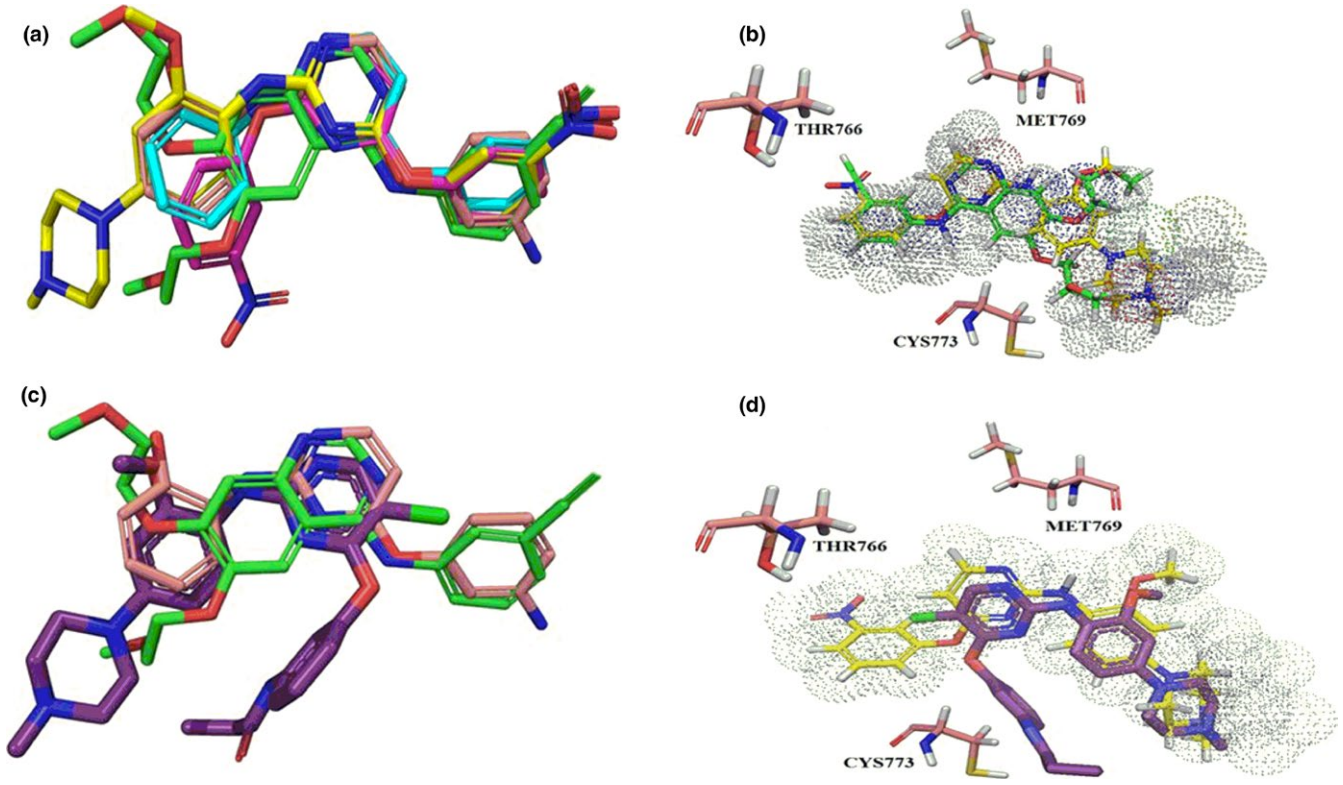


**FIGURE 4** (a) Aligned compounds **1a** (pink), **1b** (yellow), **1c** (peach) and **1d** (cyan) depicting the similar binding pattern with that of erlotinib (green); (b) 3D-interaction diagram depicting the similar binding pattern of **1b** (yellow; a representative compound) and erlotinib to the EGFR wild type; (c) Aligned compound **1d** (peach; a representative compound) and erlotinib (green) depicting the dissimilar binding pattern with that of WZ4002 (purple); (d) 3D-interaction diagram depicting the dissimilar binding pattern of **1b** (yellow; a representative compound) and WZ4002 (purple) to the EGFR wild type

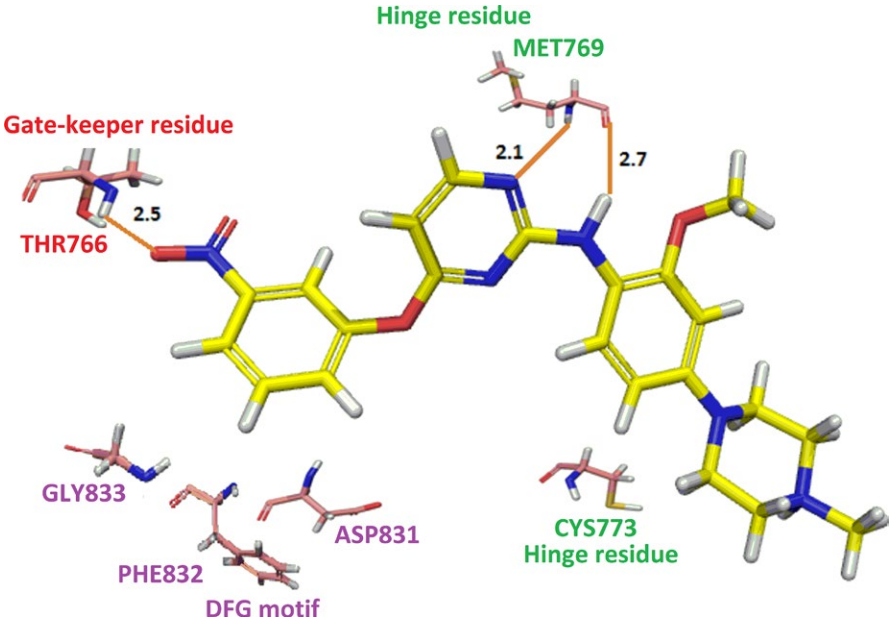


**FIGURE 5** 3D interaction diagram of **1b** depicting the important interactions with the wild-type EGFR kinase domain

(**1a–d**) along with standard EGFR inhibitors, erlotinib and WZ4002 into ATP binding site of EGFR kinase domain (PDB: 1M17)[28] was performed to theoretically understand and investigate their binding pattern. The favourable interactions between the compounds and EGFR were scored using Glide (Schrödinger Suite with MAESTRO 10.6 version). We validated the docking protocol by re-docking the erlotinib, an EGFR inhibitor, into the crystal structure of ATP binding domain of EGFR kinase domain. The docked erlotinib exhibited a binding pose similar to the co-crystallized erlotinib with a root mean square deviation of 1.27 Å which was in good agreement. It was observed that all the target compounds occupied the ATP binding site with similar binding cavity and interactions to erlotinib (Figure 4a,b). However, WZ4002 exhibited U-shaped pattern dissimilar to erlotinib and target compounds (Figure 4c,d). This supported the fact that designed compounds were reversible in nature. It was observed that **1b** and **1d** were found to have better dock score (**1b**: −7.92 and **1d**: −8.09; erlotinib: −9.02) and hence better EGFR inhibitory activity.

In spite of the different binding orientations of target compounds and erlotinib as compared to WZ4002, the pyrimidine ring of all the compounds superimposed each other and one of its nitrogen atoms and N*H* linker formed hydrogen bonds with the N$H_2$ and carbonyl oxygen atom of an important hinge region residue MET769 of the kinase ATP binding site. The hinge residues region of ATP binding site starts from the LYS764 and ends with CYS773. The other common amino acids such as GLU738, THR766, CYS773 and ASP831 were involved in the hydrogen bonding interactions whereas LEU768, GLY772 and LEU694 formed a hydrophobic pocket and participated in hydrophobic interactions with the compounds. The N$O_2$ group of **1b** was aligned towards THR766; a gatekeeper residue and involved in favourable hydrogen bonding interaction with THR766 (Figure 5). THR766 is blocked by the addition of the inhibitor while it does not participate in ATP binding. The P loop of kinase domain starts from PHE688 and ends with the TRP707. It also contains activation loop with DFG motif that contains ASP831, PHE832 and residues GLY833. The nitrophenyl ring of **1b** was surrounded by DFG motif.

**TABLE 2** Antiproliferative activity of investigational compounds **1a–d**

| | $IC_{50}$ value[a] (μM) | | |
|---|---|---|---|
| Cd | **Colon (HCT-116)** | **Breast (MCF-7)** | **Lung (A549)** |
| **1a** | 9.0 ± 0.31 | 5.1 ± 1.32 | 5.2 ± 0.54 |
| **1b** | 5.3 ± 0.74 | 4.9 ± 0.89 | 3.9 ± 0.65 |
| **1c** | 4.0 ± 0.51 | 5.2 ± 0.58 | 4.1 ± 0.44 |
| **1d** | 5.0 ± 1.1 | 3.7 ± 0.74 | 3.2 ± 0.92 |
| Erlotinib[c] | –[b] | –[b] | 2.8 ± 0.32 |

[a]Values are derived from averaging three independent experiments and each experiment was performed in triplicate.
[b]Not tested.
[c]Positive control.

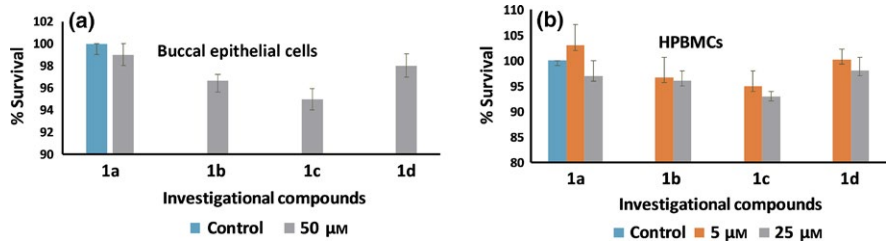


**FIGURE 6** (a) Per cent survival of buccal cavity cells at 50 µM in response to treatment with investigational compounds (**1a–d**) for a time duration of 24 hr. (b) Per cent survival of human peripheral blood mononuclear cells in response to treatment with investigational compounds (**1a–d**). Data is expressed as mean values ± *SD*. of three independent experiments

### 3.2.4 | Antiproliferative assay

To evaluate the antiproliferative potential[17,21,23] of synthetics (**1a–d**). MTT-based cell viability assay was performed using breast (MCF-7), colon (HCT-116 wild type) and lung (A549) cancer cell lines. 10,000 cells (100 µl/well) were seeded in 96 well plate and treatments with synthetics at 1, 5 and 25 µM concentration were given in triplicate followed by 24 hr incubation and thereafter analysed via MTT assay. The results are compiled in Table 2. Compound **1c** was found to exhibit $IC_{50}$ values of 4 µM in HCT-116 wild type, Compound **1d** exhibited $IC_{50}$ values of 3.7 and 3.2 µM in MCF-7 and A549 cancer cell lines, respectively. However, the compounds **1a** and **1c** were not much active against EGFR but showed comparable $IC_{50s}$ against cancer cell lines suggesting their alternate mode of anticancer mechanism(s) and not solely due to EGFR inhibition.

Further, we also evaluated the investigational compounds for their selective toxicities towards normal cells. The experiment was set using normal cells (Buccal Cavity cells) and we found no significant cytotoxicity towards normal cells even at the highest concentration of 50 µM (Figure 6a). Based on our previous research experience[17] whereby we found erlotinib possess the acute cytotoxicity to Human Peripheral Blood Mononuclear Cells (hPBMCs) at higher concentration, we were interested in evaluating our investigational compounds for their effect on hPBMCs. To our delight, we observed no significant cytotoxicity towards hPBMCs even at the highest concentration of 25 µM for 24 hr (Figure 6b).

In order to find out the anticancer effect of compounds in addition to EGFR inhibition (if any), we next planned to measure the intracellular reactive oxygen species (ROS) and alteration in mitochondrial membrane integrity of cancer cells induced by the compounds as follows.

### 3.2.5 | Dihydroethidium (DHE)-based reactive oxygen species (ROS) assay

Anticancer effects are generally associated with a change in ROS levels inside the cell.[17,21,23] To assess the effects of the synthetics on ROS level and to conclude whether the anticancer effect of the investigational compounds (**1a–d**) is mediated by free radicals, ROS assay was performed using DHE-based fluorescent detection system on lung (A549) cancer cell line.

Investigational compounds (**1a–d**) were evaluated for their ROS generation properties at 1, 5 and 25 µM concentration at 610 nm. The results showed that there is not much change in ROS levels at all concentration in comparison with positive control (Figure 7a).

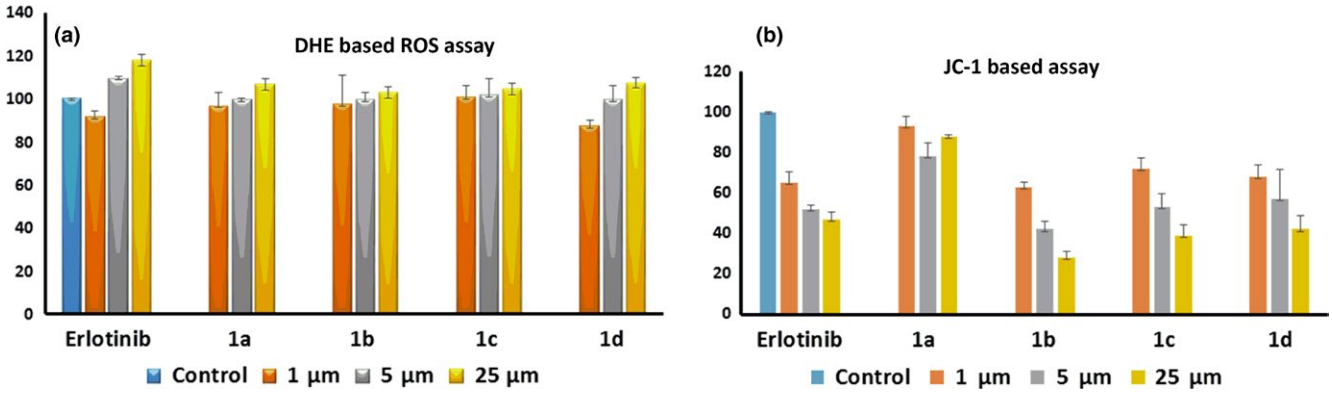


**FIGURE 7** (a) DHE-based assay to measure intracellular reactive oxygen species (ROS) induced by investigational compounds on A549 cancer cell lines. (b) JC-1 dye-based assay to measure change in mitochondrial membrane potential induced by investigational compounds on A549 cancer cell line

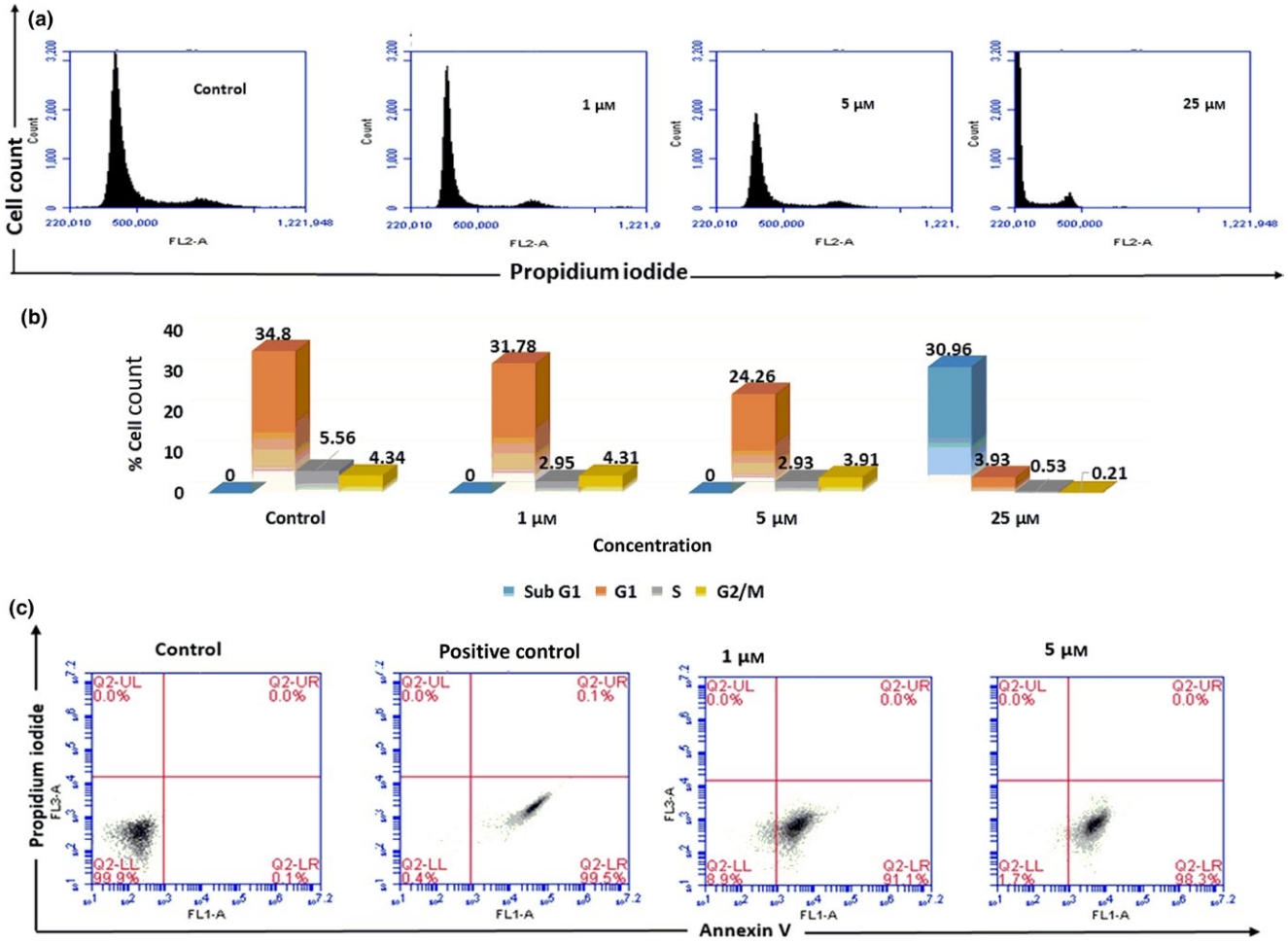


**FIGURE 8** (a) Cell cycle analysis using flow cytometry. Compound **1b** was used in the study using A549 cancer cell line (EGFR positive) that showed apoptosis (sub-G1 phase arrest). (b) The bar graph represents the per cent cell count (DNA) at various stages of cell cycle. (c) Analysis of the mode of cell death. The experiment was performed using annexin V vs propidium iodide with compound **1b** and positive control (camptothecin). The compound **1b** binds specifically to annexin V showing mode of cell death as apoptotic

### 3.2.6 | Mitochondrial membrane integrity (JC-1) assay

During programmed cell death several key events occur in mitochondria amongst which mitochondrial transmembrane potential is an important parameter that defines the fate of cancer cells. Anticancer drugs are known to cause variation in mitochondrial potential which is easily detected by cytofluorimetric dyes.[17,21,23] Deviations in mitochondrial membrane potential lead to the release of cytochrome-c into cytoplasm thus induce intrinsic pathway of apoptosis. To investigate the changes in mitochondrial membrane induced by the synthetic molecules (**1a–d**; at 1, 5 and 25 μM concentration) were assayed on A-549 lung cancer cells using lipophilic cationic dye, 5,5′,6,6′-tetrachloro-1,1′,3,3′tetraethylbenzimi-dazolylcarbocyanine iodide (JC-1). JC-1 dye selectively enters mitochondria and reversibly changes colour from red to green as membrane potential decreases (OD590/OD527 ratio). The results showed that all the compounds lead to imbalance OD590/527 ratios and thus destabilize mitochondrial membrane (Figure 7b) which in turn, leads to cytochrome-c leakage to the cytoplasm. Cytochrome-c leakage into the cytoplasm is one of the foundation steps during initiation of apoptosis.

### 3.2.7 | Cell cycle analysis and mode of cell death

Anticancer compounds tend to cause cell death and delay the cell cycle progression by arresting cell cycle.[17,21] To investigate the specific phase of inhibition, A549 cell line was treated with a selected compound **1b** at 1, 5 and 25 μM concentrations for 24 hr. The results showed no significant changes in G1, S as well as G2–M phases, but it was observed that sub-G1 population increased several folds at higher concentration of the **1b** (0%–30%) indicative of cell death. It may be hypothesized that the drug may be toxic to

the cells independent of the status of the cell cycle as it is evident from the Figure 8a that G1, S and G2–M phases showed very less number of cells at a higher dose of the drug compared to the profiles observed in control cells (Figure 8b). Another possible explanation is that these cancer cells might be having mitotic catastrophy[33] at higher drug concentrations. So, to confirm the mode of cell death, we went on to perform annexin V as well propidium iodide staining at the same concentrations. Annexin V positive cells indicate apoptotic populations while under normal conditions, propidium iodide does not stain live or early apoptotic cells due to the existence of an undamaged plasma membrane. In late apoptotic and necrotic cells, the integrity of the plasma and nuclear membranes declines to allow propidium iodide to pass through the membranes which further intercalate into nucleic acids and display red fluorescence. Whether the investigational compound **1b** exhibited early apoptosis or the mode of cell death was late apoptosis/necrosis the experiment was setup using A549 cell line in conjugation with propidium iodide and annexin V. This experiment detects the release of phosphatidylserine and its conjugation with annexin V dye. The result exhibited that the mode of cell death was apoptosis (early apoptosis) as seen by annexin V binding to early apoptosis quadrant in (Figure 8c). Camptothecin was taken as positive control for the study at a concentration of 10 μM.

## 4 | CONCLUSION

In summary, we have designed, synthesized and evaluated the pyrimidine-based compounds (**1a**–**1d**) for their potential to exhibit anti-EGFR kinase activity at nanomolar range (**1b** and **1d**) and anticancer activity at the low micromolar range. The above observations were further supported by the facts that they were able to alter the levels of EGFR downstream targets and mitochondrial membrane potential leading to the initiation of apoptosis of cancer cells. However, compounds were not able to alter the intracellular ROS levels of cancer cells. Molecular docking studies revealed that compounds could align in the ATP binding pocket of EGFR similar to erlotinib but dissimilar to WZ4002. Annexin V versus propidium iodide-based assay suggested that mode of cell death was due to apoptosis. All the above observations indicated multiple modes of mechanisms involved in anticancer effects of compounds. Further results on their detailed antitumor potential will be published in due course.

## ACKNOWLEDGMENT

RK and GJ thank UGC, New Delhi, India for the financial assistance F.30-13/2013(BSR). SS thanks DST for financial assistance (DST-SERB EMR, SR/SO/AS-31/2014), PS is the recipient of JRF from the project.

## CONFLICT OF INTEREST

The authors declare no conflict of interest.

## REFERENCES

[1] G. Joshi, P. K. Singh, A. Negi, A. Rana, S. Singh, R. Kumar, *Chem. Biol. Interact.* **2015**, *240*, 120.
[2] D. Hanahan, R. Weinberg, *Primer of the Molecular Biology of Cancer, 2nd ed., Wolters Kluwer, Philadelphia,* **2015**, 28-57.
[3] J. A. McCubrey, S. L. Abrams, T. L. Fitzgerald, L. Cocco, A. M. Martelli, G. Montalto, M. Cervello, A. Scalisi, S. Candido, M. Libra, *Adv. Biol. Regul.* **2015**, *57*, 75.
[4] S. Seton-Rogers, *Nat. Rev. Cancer* **2016**, *16*, 128.
[5] A. L. Hopkins, *Nat. Chem. Biol.* **2008**, *4*, 682.
[6] P. Seshacharyulu, M. P. Ponnusamy, D. Haridas, M. Jain, A. K. Ganti, S. K. Batra, *Expert Opin. Ther. Targets* **2012**, *16*, 15.
[7] A. Russo, T. Franchina, G. Ricciardi, A. Picone, G. Ferraro, M. Zanghì, G. Toscano, A. Giordano, V. Adamo, *Oncotarget* **2015**, *6*, 26814.
[8] D. W. Bell, I. Gore, R. A. Okimoto, N. Godin-Heymann, R. Sordella, R. Mulloy, S. V. Sharma, B. W. Brannigan, G. Mohapatra, J. Settleman, *Nat. Genet.* **2005**, *37*, 1315.
[9] T. K. Sundaresan, L. V. Sequist, J. V. Heymach, G. J. Riely, P. A. Jänne, W. H. Koch, J. P. Sullivan, D. B. Fox, R. Maher, A. Muzikansky, *Clin. Cancer Res.* **2016**, *22*, 1103.
[10] S. M. Lim, Y. Jeong, S. Hong, *Future Med. Chem.* **2016**, *8*, 853.
[11] I. Stasi, F. Cappuzzo, *Transl. Respir. Med.* **2014**, *2*, 1.
[12] J. Engel, J. Lategahn, D. Rauh, *ACS Med. Chem. Lett.* **2015**, *7*, 2.
[13] S. L. Greig, *Drugs* **2016**, *76*, 263.
[14] Z. Song, Y. Ge, C. Wang, S. Huang, X. Shu, K. Liu, Y. Zhou, *J. Med. Chem.* **2016**, *59*, 6580.
[15] L. Landi, F. Cappuzzo, *Transl. Lung Cancer Res.* **2013**, *2*, 40.
[16] J. M. Alex, S. Singh, R. Kumar, *Arch. Pharm.* **2014**, *347*, 717.
[17] M. Chauhan, G. Joshi, H. Kler, A. Kashyap, S. M. Amrutkar, P. Sharma, K. D. Bhilare, U. C. Banerjee, S. Singh, R. Kumar, *RSC Adv.* **2016**, *6*, 77717.
[18] M. Chauhan, A. Rana, J. M. Alex, A. Negi, S. Singh, R. Kumar, *Bioorg. Chem.* **2015**, *58*, 1.
[19] G. Kaur, R. P. Cholia, A. K. Mantha, R. Kumar, *J. Med. Chem.* **2014**, *57*, 10241.
[20] A. Kondaskar, S. Kondaskar, R. Kumar, J. C. Fishbein, N. Muvarak, R. G. Lapidus, M. Sadowska, M. J. Edelman, G. M. Bol, F. Vesuna, *ACS Med. Chem. Lett.* **2010**, *2*, 252.
[21] R. Kumar, U. C. Banerjee, S. M. Amrutkar, A. T. Baviskar, S. Singh, G. Joshi, H. Kler, *RSC Adv.* **2016**, *6*, 14880.
[22] S. Kumar, S. Sapra, R. Kumar, M. K. Gupta, S. Koul, T. Kour, A. K. Saxena, O. P. Suri, K. L. Dhar, *Med. Chem. Res.* **2012**, *21*, 3720.
[23] A. Negi, J. M. Alex, S. M. Amrutkar, A. T. Baviskar, G. Joshi, S. Singh, U. C. Banerjee, R. Kumar, *Bioorg. Med. Chem.* **2015**, *23*, 5654.
[24] A. Rana, J. M. Alex, M. Chauhan, G. Joshi, R. Kumar, *Med. Chem. Res.* **2015**, *24*, 903.
[25] Y. Sakuma, Y. Yamazaki, Y. Nakamura, M. Yoshihara, S. Matsukuma, H. Nakayama, T. Yokose, Y. Kameda, S. Koizume, Y. Miyagi, *Lab. Invest.* **2012**, *92*, 371.
[26] Z. Li, X. Li, X. Gao, Y. Zhang, W. Shi, H. Ma, *Anal. Chem.* **2013**, *85*, 3926.
[27] J. Linam, L.-X. Yang, *Anticancer Res.* **2015**, *35*, 2479.

[28] J. Stamos, M. X. Sliwkowski, C. Eigenbrot, *J. Biol. Chem.* **2002**, *277*, 46265.
[29] H. Babich, M. Krupka, H. A. Nissim, H. L. Zuckerbraun, *Toxicol. In Vitro* **2005**, *19*, 231.
[30] J. H. Weisburg, D. B. Weissman, T. Sedaghat, H. Babich, *Basic Clin. Pharmacol. Toxicol.* **2004**, *95*, 191.
[31] C. Han, L. Wan, H. Ji, K. Ding, Z. Huang, Y. Lai, S. Peng, Y. Zhang, *Eur. J. Med. Chem.* **2014**, *77*, 75.
[32] L.-Y. Hung, J. T. Tseng, Y.-C. Lee, W. Xia, Y.-N. Wang, M.-L. Wu, Y.-H. Chuang, C.-H. Lai, W.-C. Chang, *Nucleic Acids Res.* **2008**, *36*, 4337.
[33] M. Castedo, J.-L. Perfettini, T. Roumier, K. Andreau, R. Medema, G. Kroemer, *Oncogene* **2004**, *23*, 2825.

## SUPPORTING INFORMATION

Additional Supporting Information may be found online in the supporting information tab for this article.

**How to cite this article:** Joshi G, Nayyar H, Kalra S, et al. Pyrimidine containing epidermal growth factor receptor kinase inhibitors: Synthesis and biological evaluation. *Chem Biol Drug Des*. 2017;00:1–12. https://doi.org/10.1111/cbdd.13027